

Article

Capacity Fade in Lithium-Ion Batteries and Cyclic Aging over Various State-of-Charge Ranges

Sophia Gantenbein ^{*}, Michael Schönleber, Michael Weiss and Ellen Ivers-Tiffée

Institute for Applied Materials (IAM-WET), Karlsruhe Institute of Technology (KIT), 76131 Karlsruhe, Germany; michael.schoenleber@bafemo.de (M.S.); m.weiss@kit.edu (M.W.); ellen.ivers@kit.edu (E.I.-T.)

* Correspondence: sophia.gantenbein@kit.edu; Tel.: +49-721-608-47565

Received: 10 October 2019; Accepted: 18 November 2019; Published: 26 November 2019



Abstract: In order to develop long-lifespan batteries, it is of utmost importance to identify the relevant aging mechanisms and their relation to operating conditions. The capacity loss in a lithium-ion battery originates from (i) a loss of active electrode material and (ii) a loss of active lithium. The focus of this work is the capacity loss caused by lithium loss, which is irreversibly bound to the solid electrolyte interface (SEI) on the graphite surface. During operation, the particle surface suffers from dilation, which causes the SEI to break and then be rebuilt, continuously. The surface dilation is expected to correspond with the well-known graphite staging mechanism. Therefore, a high-power 2.6 Ah graphite/LiNiCoAlO₂ cell (Sony US18650VTC5) is cycled at different, well-defined state-of-charge (SOC) ranges, covering the different graphite stages. An open circuit voltage model is applied to quantify the loss mechanisms (i) and (ii). The results show that the lithium loss is the dominant cause of capacity fade under the applied conditions. They experimentally prove the important influence of the graphite stages on the lifetime of a battery. Cycling the cell at SOCs slightly above graphite Stage II results in a high active lithium loss and hence in a high capacity fade.

Keywords: cyclic aging; capacity fade; active lithium loss; graphite staging mechanism; graphite particle dilation; open circuit voltage model

1. Introduction

The investigation of degradation mechanisms in lithium-ion batteries has proven essential for increasing the service life and extending operation. Full understanding of these mechanisms enables actions to reduce and mitigate degradation. In addition, a longer service life of the batteries used leads to less frequent replacement in the application. This reduces resource consumption and contributes to greater sustainability. One consequence of degradation is capacity fade, which can lead to declines in device usability.

Capacity fade is caused by a loss of active electrode material (loss of storage medium): For example, if the cathode material becomes unstable at high potentials, it can no longer store lithium [1,2]. Pressingly, recent studies have shown that the loss of active electrode material is actually low compared to the loss of active lithium (loss of storage content) [3]. Two main mechanisms cause active lithium loss.

Graphite is currently the most commonly used active anode material. Active lithium can get lost due to irreversible plating or the formation of a solid electrolyte interface (SEI) on the graphite surface [4,5]. While plating can be reduced by applying an optimized charge process [6], SEI formation on the graphite particle surface is inevitable and even desirable. Liquid electrolytes for lithium-ion batteries are not stable below a potential of 1.5 V vs. Li. They decompose at the graphite surface to form an ion-conducting surface film called SEI, which protects the electrolyte against further decomposition [7]. Lithium is consumed in these decomposition reactions [8].

However, the SEI is not only built at the beginning of life (BOL) of the battery. During operation (i.e., during deintercalation and intercalation of lithium), the electrode particles suffer from volume changes and mechanical stresses. The volume change is negligible for LiCoO_2 -based cathode materials [9] but can be up to 10% for graphite [4,10]. The dilation of the graphite particle surface causes the SEI to break. This exposes fresh graphite surface on which new SEI is built. Hence, lithium is consumed continuously due to volume changes of the particle surface during operation and the cell progressively loses capacity.

The intercalation of lithium into the graphite particle layers follows a clear staging mechanism [11,12]. This is schematically shown in Figure 1. In Stage IV, every fourth layer of the graphite structure is fully lithiated. With further lithiation, Stage III is formed, which means that every third layer is now lithiated. Hence, from Stage IV to Stage III, one additional layer out of twelve is opened. The transition from Stage III to Stage II comes along with two additional layers out of twelve being opened, whereas the final transition from Stage II to Stage I requires six additional layers out of twelve to be opened. Each time a new layer is opened, the graphite particle widens at the edge and the SEI is expected to break. Then, the SEI will cover the fresh surface, further depleting the available lithium.

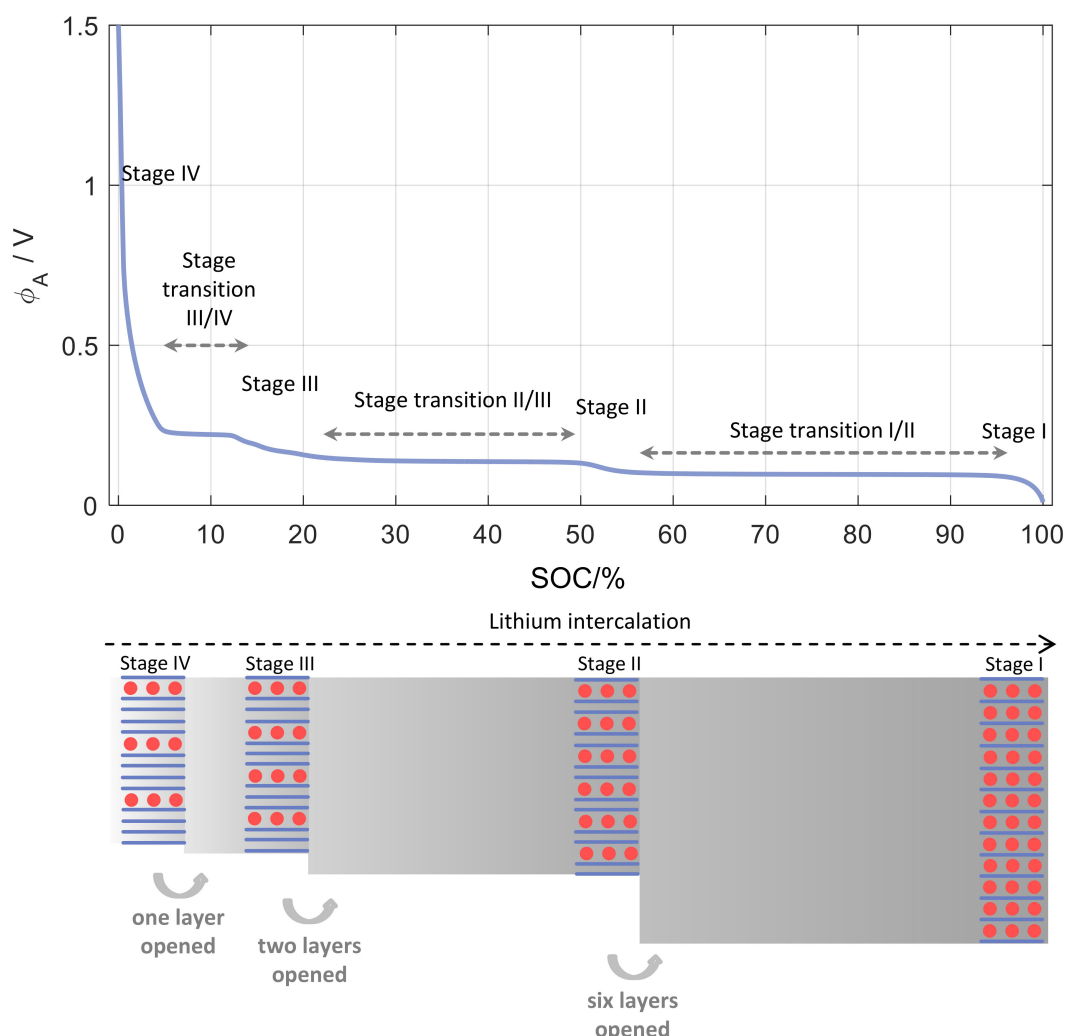


Figure 1. Graphite potential and schematic lithium intercalation during charging. The transition from Stage IV to Stage III requires one out of twelve layers to be opened, the transition from Stage III to Stage II requires two out of twelve layers to be opened, and the transition from Stage II to Stage I requires six out of twelve layers to be opened.

Therefore, when operating a lithium-ion cell with a graphite anode in different SOC ranges, the capacity loss caused by the loss of active lithium (due to the SEI breaking and rebuilding) is expected to be greatest in the range of Stage II when Stage I is being opened. This is the point of highest risk. The transition from Stage II to Stage I was also modeled in [13]. The experimental investigation of this hypothesis is the focus of this work. For this reason, five different cycle-life experiments were conducted, in which the cells were cycled across different ranges of the anode potential. The capacity loss of the commercial full cell was determined at regular intervals during aging. To quantify the active lithium loss, a nondestructive method was applied, based on an open circuit voltage (OCV) model. The model simulates the full-cell OCV by the difference between the cathode and the anode open circuit potential (OCP) [14,15]. The cause of capacity loss can be determined with a little additional experimental effort. A single commercial cell does have to be opened, and both electrode potentials are measured in experimental cells. This data set is then available for use in the OCV model at all times (and means that other cells need not be disassembled). In [15], it was already demonstrated that the model is applicable for the investigation of cell degradation. The approach was recently applied in [16,17] to analyze the degradation mechanisms in a lithium-ion battery. Further, this study is the first time the model has been used to systematically investigate the influence of the graphite potential and its stages on the capacity loss of a lithium-ion battery.

2. Experimental Section

2.1. Investigated Cell

This study investigated a high-power 18650 lithium-ion cell with a nominal capacity of 2.6 Ah (Sony US18650VTC5). The Sony VTC5 is a popular cell, ideal for modern power tools. The upper and lower voltage limits were 4.2 and 2.5 V, the maximum charge and discharge currents were 4 (approx. 1.5 C-rate) and 20 A (approx. 8 C-rate). The cell is composed of graphite as anode material and LiNiCoAlO₂ and carbon black as cathode material.

2.2. Experimental Cells

To obtain the cathode and anode OCP, the 18650 cell was discharged to 2.5 V by a current rate of C/2 and afterwards opened and disassembled in an argon filled glovebox. In the next step, experimental half-cells with a diameter of 18 mm were built with a lithium counter electrode (Sigma-Aldrich, product number 265985, 99.9% trace metals basis). The experimental cell housings ECC-PAT-Core (EL-CELL) are equipped with a lithium reference electrode. The liquid electrolyte was a 1 mol/L⁻¹ LiPF₆ solution in a 1:1 mixing ratio of ethylene carbonate:dimethyl carbonate (BASF, Selectlyte LP30). The two experimental cells were built with anode and cathode material, respectively, and the half-cell potentials were recorded against the reference electrode with a C/40-rate (175 µA) from 0.05 to 1.5 V (anode) and from 4.4 to 3.0 V (cathode).

2.3. Analytical Equipment

The cycle-life aging tests were performed using a Basytec XCTS cell test system with 25 A maximum output current. According to the technical data-sheet, this system has a current precision of 50 mA (see Table 1). Since the capacity measurements in the characterization tests and the experimental cell measurements require small currents (65 and 175 µA) and high precision, these tests were performed using a Basytec CTS-LAB cell test system with 3 A maximum output current. This system has a current precision of 50 and 0.2 µA in the required current ranges.

All measurements were carried out at a constant temperature of 25 °C. For this reason, the cells were placed in a Friocell 55 climate chamber from MMM Medcenter Einrichtungen GmbH (0.0–99.9 °C). The climate chamber has a temporal temperature accuracy of ±0.2 °C and a spatial temperature accuracy of ±0.5 °C. All cells were tested simultaneously in the same climate chamber, and the temperature was continuously monitored.

Table 1. Technical specifications of the Basytec XCTS and CTS-LAB systems.

	Basytec XCTS	Basytec CTS-LAB
current range	25 A	3 A/250 mA/15 mA/1 mA
current precision	50 mA up to 25 A	500 μ A/50 μ A/2.5 μ A/0.2 μ A
current resolution	1 mA	100 μ A/8 μ A/0.5 μ A/0.05 μ A

2.4. Test Procedure

After the initial characterization at BOL, the cells were cycled for 4000 cycles with 20% depth of discharge (Δ DOD), which results in a total charge throughput of 4160 Ah. At the end of the cycle life test (EOT), a final characterization was conducted. Interim checkups were performed at intervals of every 500 cycles to assess cell aging and to readjust the SOC ranges over which the cells were cycled. Two cells were tested under the same conditions to ensure result reproducibility.

2.4.1. Characterization Tests

The remaining cell capacity was determined by conducting a standard charge until 100% SOC (C/2-rate constant current charge to 4.2 V, constant voltage charge at 4.2 V until the current decreased below 100 mA), and then discharging to 0% SOC (2.5 V). At BOL and EOT, the actual capacity was measured by discharging the cell with a C/40-rate (65 mA). After each 500 cycles, the actual capacity was measured by discharging the cell with a C/10-rate (260 mA) due to time constraints. The low current rate in the capacity measurements allowed us to measure the actual capacity fade. A capacity measurement at higher C-rates could have distorted the capacity fade: Higher losses during discharge could have caused the lower voltage limit to be reached earlier, and the measurement result does not reflect the actual capacity. This effect was further reinforced during aging because the inner resistance of the cell increased. In addition, the low discharge rate ensured near-equilibrium conditions, which was a prerequisite for the application of the OCV model (see Section 2.5).

2.4.2. Cycle-Life Tests

Cycle-life tests were performed following the information detailed in Table 2 and Figure 2. The focus of this test matrix was the influence of the SOC range (i.e., the graphite potential and its stages) on the loss of active lithium. As explained in the introduction, a higher capacity loss is expected in the range of Stage II when Stage I is opening. Figure 2 shows the quasi-OCV $V_{OCV,full}$ of the Sony VTC5 full cell (black line; recorded with a C/40-rate) and the corresponding anode potential φ_A (blue line). Since the anode is usually oversized compared to the cathode, the fully lithiated state of the anode is not reached at a full cell SOC of 100%. The differential voltage, DV_{full} , of the full cell OCV is plotted (grey line) to clearly indicate the position of Stage II at a full cell SOC of 55%. The differential voltage is defined by:

$$DV(Q) = dQ/dU \quad (1)$$

and allows us to better visualize the electrode features. In addition to the graphite stages, the LiNiCoAlO₂ cathode feature is visible at a full cell SOC of 85%. The choice of SOC ranges for cycling was motivated as follows:

- To ensure the cycling in an SOC range which fully passes Stage II, the first SOC range was set to 45–65%;
- The charge throughput should not vary, which means all experiments passed a Δ DOD of 20%. Ideally, the whole SOC range (0–100%) should be covered, which requires five different SOC ranges;
- The SOC ranges 25–45% and 65–85% covered the plateau regions (stage transitions) of the graphite anode. In theory, they should not pass any stages.

Cycling up to 100% and down to 0% SOC was not possible because of the system loss and the resulting overvoltage. The upper and lower voltage limits of 4.2 and 2.5 V would be reached before 100% and 0%

SOC could be realized. Hence, the highest and lowest possible SOC ranges were 75–95% and 5–25%. For the investigation in this study, it was of great importance to prevent SOC drifts and to ensure that the cells were always cycled over the same SOC ranges. For this reason, the SOC ranges were adjusted as follows:

- At the beginning of each 500 cycles, the cell was charged to 100% SOC with the method explained in Section 2.4.1 and then discharged with a 1C-rate until the upper limit of the intended SOC range by Ah-counting. For example, if the cell was supposed to be cycled in the SOC range 65–85%, 15% of the actual cell capacity was discharged to reach the upper SOC limit of 85%. Hence, at BOL, when the cell had a capacity of 2.6 Ah, $Q_{15,BOL} = 0.15 \cdot 2.6 \text{ Ah} = 0.39 \text{ Ah}$ was discharged.
- As the cells lost capacity, this value needed to be adjusted to the actual remaining capacity. Hence, for the cell cycled in the SOC range 65–85%, $Q_{15,\text{remaining}} = 0.15 \cdot Q_{\text{remaining}}$ was discharged after each interim checkup to adjust the upper limit of the intended SOC range.
- Depending on the causes of capacity loss (active lithium loss, active electrode material loss), the position of the electrode potentials in the full cell changes. To ensure that the cells were always cycled over the same range of the anode potential, a differential voltage analysis was performed in each checkup. If the position of Stage II of the graphite anode changed significantly, this would necessitate further adjustments of the upper limit of the intended SOC range.
- After the adjustment of the upper SOC limit and a 10 min respite, the cell was discharged with 10 A and charged with 2.5 A for five cycles with 20% ΔDOD by Ah-counting. A total of 20% ΔDOD always refers to the initial capacity of the cell at BOL, which means charge/discharge of 520 mAh. In this manner, all cells had the same total charge throughput during aging. During these first five cycles, the mean values of the lower and upper terminal voltage were calculated. In the remaining 495 cycles, the cell was discharged and charged between these voltage limits.

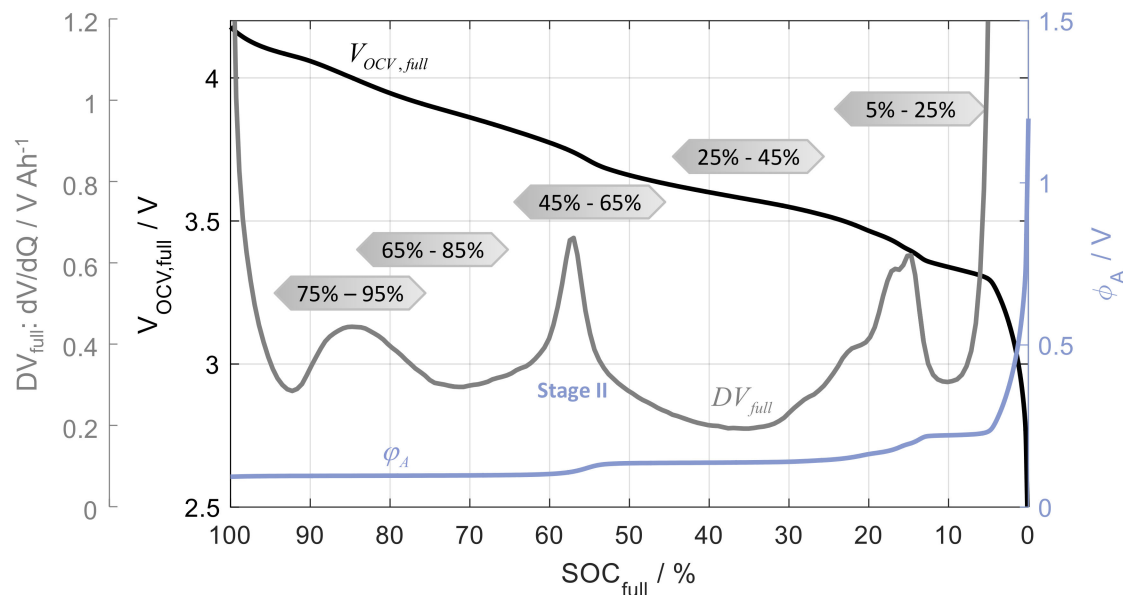


Figure 2. State of charge (SOC) ranges of the cycle-life tests with regard to the full cell open circuit voltage (OCV), $V_{OCV,full}$, and the corresponding open circuit potential (OCP) of the graphite anode, ϕ_A . The differential voltage, DV_{full} , calculated from $V_{OCV,full}$ clearly indicates the position of Stage II at a full cell SOC of 55%.

Table 2. Cycle-life tests.

T/°C	25
discharge current/A	10
charge current/A	2.5
SOC range/%	5–25 25–45 45–65 65–85 75–95

2.5. Data Analysis

During aging, the battery either lost capacity due to active lithium loss (ALL) or to active material loss of the anode (AML_A) or the cathode (AML_C) [1]. These losses can be separated and quantified nondestructively with the help of an OCV model [14,15]. The underlying model (represented in Figure 3) is based on the calculation of the full cell OCV, $V_{OCV,full}$, by the difference between the cathode OCP, φ_C , and the anode OCP, φ_A :

$$V_{OCV,full}(Q) = \varphi_C(Q) - \varphi_A(Q) \quad (2)$$

The OCV model scales the OCPs of the electrodes and aligns them in such a way that their difference correctly resembles the full cell OCV. This is explained in detail in [14,15]. During aging, the shape of the full cell OCV changes due to ALL and AML_A/AML_C . To describe the OCV of an aged cell, the electrodes' OCP has to be shifted by a shift factor v_A/v_C and scaled by a scaling factor α_A/α_C compared to BOL [15]:

$$V_{OCV,full}(Q) = \varphi_C(\alpha_C \cdot Q - v_C) - \varphi_A(\alpha_A \cdot Q - v_A) \quad (3)$$

This approach is shown in Figure 4. When active lithium is lost, the electrodes' OCP have to be shifted against each other; if the anode OCP is shifted to the left compared to the cathode OCP, neither electrode can be lithiated to the same degree as before within the full cell voltage limits of 2.5–4.2 V. At BOL, the anode is delithiated when $Q_{A,1}$ is discharged from the fully charged cell. When active lithium is lost, the cathode is not fully lithiated, when the anode is delithiated and the anode OCP shifts to the left compared to the cathode OCP. Then, the anode is delithiated when $Q_{A,2}$ is discharged from the fully charged cell. The loss of active lithium can hence be calculated from the difference:

$$ALL = Q_{A,1} - Q_{A,2} \quad (4)$$

If active electrode material is lost, the storage capacity shrinks and the OCP of the respective electrode has to be scaled. At BOL, the cathode OCP ranges from 0 to $Q_{C,1}$. When active cathode material is lost, the cathode cannot take the same amount of lithium as before and the cathode OCP ranges from 0 to only $Q_{C,2}$. The loss of active material hence results in:

$$AML_C = Q_{C,1} - Q_{C,2} \quad (5)$$

The same holds for the loss of active anode material. The full cell capacity loss is not determined by the sum of the individual losses ALL, AML_A , and AML_C . Instead, only one of the three losses is the limiting factor and dominantly determines Q_{loss} . For example, if the remaining lithium inventory is sufficient to lithiate 50% of the electrode, a reduction of active electrode material from 100% down to 50% does not cause any further capacity loss in the full cell. As shown in Figure 4, active lithium loss dominantly determines the remaining full cell capacity.

Since Equation (2) is only valid at equilibrium, all curves used in this model had to be obtained with low current rates to ensure near-equilibrium conditions. The electrodes' OCPs were measured at BOL and this data set was used to analyze all aged full cells. For use with the OCV model, the electrodes' capacities (electrode area of 2.54 cm^2) were normalized to the 18,650 full cell (electrode area of 912 cm^2).

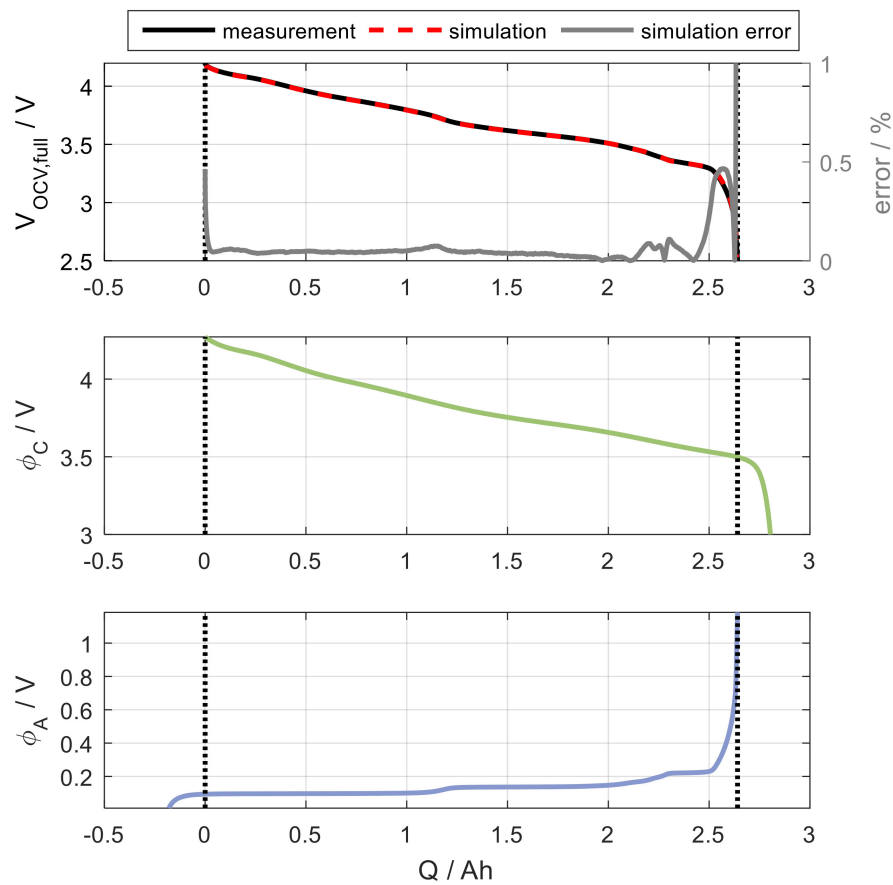


Figure 3. OCV model for the Sony VTC5 cell at beginning of life (BOL), the full cell OCV, $V_{OCV,full}$, (**top**) is simulated by the difference of the cathode OCP, φ_C , (**middle**) and the anode OCP, φ_A , (**bottom**).

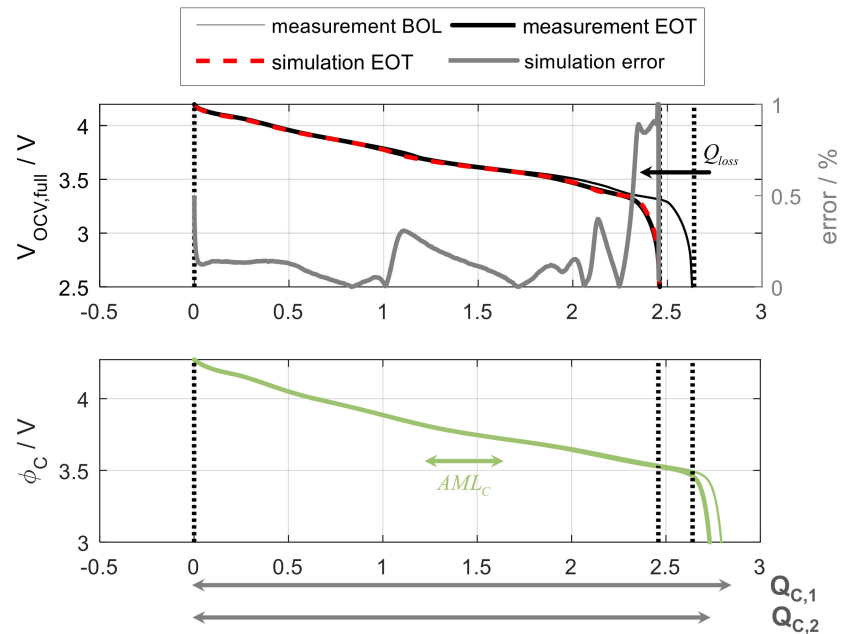


Figure 4. Cont.

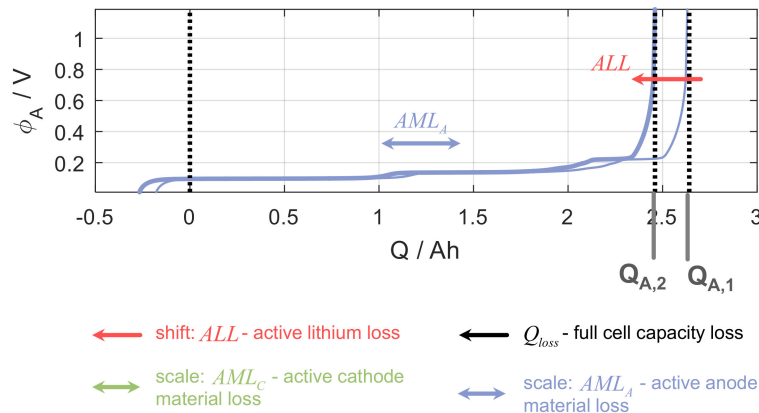


Figure 4. OCV model for the Sony VTC5 cell at BOL and at end of cycle life test (EOT) for the cell cycled over the SOC range 75–95%. Active lithium loss requires a shift of the electrodes' OCPs against each other. Active material loss requires a scaling of the electrodes' OCPs.

3. Results

Figure 5a shows the full cell capacity loss at EOT for each cycle-life test. The capacity loss first increased with increasing mean SOC, reached its maximum value in the SOC range 65–85%, and decreased again for the SOC range 75–95%. Figure 5b shows the individual capacity loss contributions. In each cycle-life test, the full cell capacity loss was determined by the loss of active lithium, ALL. Neither the loss of active anode material, AML_A , nor of active cathode material, AML_C , influenced the full cell capacity loss at this stage of degradation. The fit results determined that active lithium loss was slightly higher than the full cell capacity loss, which is physically not possible. This is a systematic effect which can be easily explained: During aging, the anode potential shifts to the left compared to the cathode potential. Hence, when the anode is fully delithiated, the corresponding cathode potential is higher at EOT than at BOL. As a result, the lower cut-off voltage of the full cell is reached later and the actual capacity that can be measured is higher. This effect is not considered in the OCV model; however, the difference is negligible. Figure 5c–g shows the courses of the individual capacity loss contributions of the respective cell from cycle 1500 to EOT. Slight deviations between the results in Figure 5b compared against the results in Figure 5c–g arise from the use of C/40 discharge curves in the OCV model at BOL and EOT, and the use of C/10 discharge curves for the interim checkups. With increasing current, the electrodes' features are less clearly identifiable, and the OCV model delivers slightly different results. However, the difference in the full cell capacity loss was close to zero when measuring the capacity with a C/40- and with a C/10-rate. This justifies the use of C/10-rates when analyzing the capacity loss. As already reported in [18], the capacity loss rate shown in Figure 5c–g tended to decrease with time.

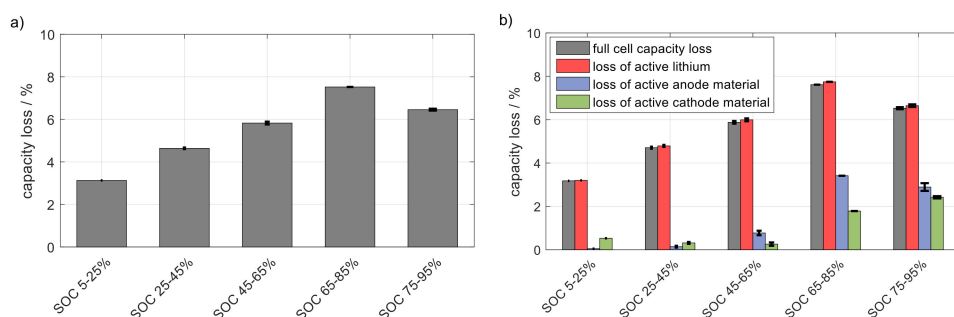


Figure 5. Cont.

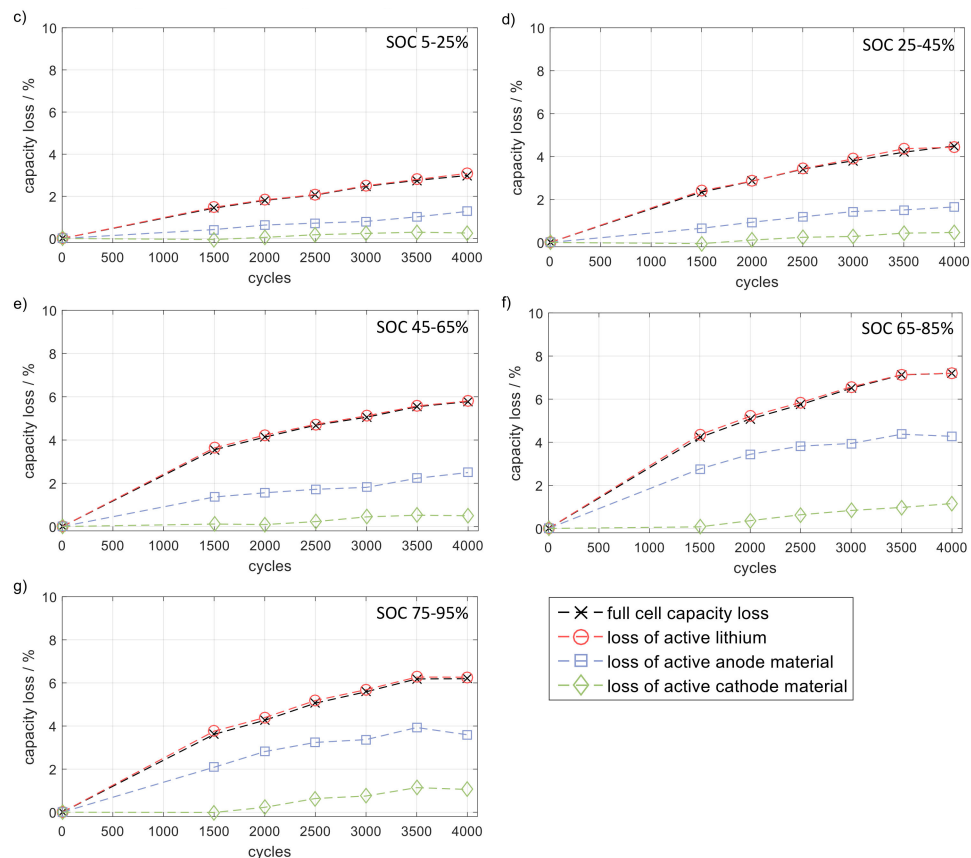


Figure 5. (a) Full cell capacity loss for each cycle-life test, measured at EOT by discharging the cell with a C/40-rate. The results represent the mean value of two cells tested under the same conditions; error bars indicate the deviation. (b) Q_{loss} , active lithium loss (ALL), active material loss of the anode (AML_A), and of the cathode (AML_C) for each cycle-life test. The results were obtained with the OCV model at EOT using C/40 discharge curves. The results represent the mean value of two cells tested under the same conditions; error bars indicate the deviation. (c–g) Courses of Q_{loss} , ALL, AML_A , and AML_C for each cycle-life test over the lifetime of the cell. The results were obtained with the OCV model at each interim checkup using C/10 discharge curves and represent the mean value of two cells tested at the same conditions.

4. Discussion

4.1. Interpretation of Active Lithium Loss, ALL, and Active Anode Material Loss, AML_A

As explained in the introduction, six final graphite layers out of twelve need to be opened at Stage II to further lithiate the anode. The highest relative dilation of the particle surface was therefore expected at Stage II. Cycling the cell over an SOC range which includes this stage should result in SEI cracking, SEI rebuilding, and active lithium loss. Additionally, if active anode material was lost by particle cracking, this was also expected to happen when the particles suffer from mechanical stress. Intuitively, one would expect the loss of active lithium, ALL, as well as the loss of active anode material, AML_A , to be greatest for the cell cycled in the SOC range 45–65% which includes Stage II at an SOC of 55%. However, the cell cycled over the SOC range 65–85% showed the most ALL, followed by the cell cycled over the SOC range 75–95%. The loss of active anode material, AML_A , showed a qualitatively similar dependency.

A drift of the SOC range during aging where the cells would not always be cycled in the same range of the anode potential would distort the results. Such drifts were prevented by the adjustment of the SOC ranges, explained in Section 2.4.2. Figure 6 proves the correct implementation of the cycle-life experiments. Figure 6a shows the differential voltage of the C/40 discharge curves at BOL and at EOT

for all cycle-life tests, plotted over the capacity, where the last point on the x-axis indicates the remaining capacity. Since the SOC ranges were adjusted to the actual remaining capacity of the respective cell during aging, the differential voltage curves needed to be normalized to see whether the position of Stage II shifted significantly with regard to the SOC. As this is not the case (see Figure 6b), the resulting capacity losses were not distorted by an erroneous implementation of the aging experiments.

The peak in the differential voltage at approx. 85% SOC originates from the LiNiCoAlO₂ cathode. However, the suggestion that this cathode feature could be an explanation for the high loss of active lithium in the cells cycled in the SOC ranges 65–85% and 75–95% does not stand up to scrutiny. Firstly, the cell cycled in the SOC range 75–95% did not lose more active lithium than the cell cycled in the SOC range 65–85%, even though it fully passed the cathode feature. Secondly, the loss of active anode material qualitatively corresponded with the loss of active lithium, which hints that the active lithium loss occurred due to particle dilation at the anode side. Thirdly, there are no references in literature which show a direct connection between active lithium loss and the LiNiCoAlO₂ cathode feature.

One explanation for these results is: A graphite particle will not open all six “final” layers simultaneously at Stage II (at a full cell SOC of 55%), but in such a way as to reach a favorable energetic state.

- When reaching an SOC of 55% during lithiation, the first of these “final” particle layers will open, and lithium will begin to diffuse into these layers towards the particle interior. When cycling in the SOC range 45–65%, only these few layers close and open again and contribute to the dilation of the particle surface. This is schematically shown in Figure 7d. The representation of the particle must not be interpreted as a cross-section, but figuratively: Only a small surface area fluctuates between Stage I (dark blue) and Stage II (medium blue) in each cycle. The actual part of the particle surface which expands is indicated by the red line;
- With increasing lithiation, more “final” layers will open. At a certain point between an SOC of 55% and 100%, the number of layers that close and open again during cycling is maximal. Hence, the SEI cracks and the corresponding loss of active lithium is maximal. This is the case for the SOC range 65–85%, shown in Figure 7c. The area in dark blue at an SOC of 65% represents those layers which will always remain open during cycling (because they always contain lithium) and will not cause further particle surface expansion. This area is comparatively small. Conversely, the surface area which fluctuates between Stage I and Stage II in each cycle is high;
- With further lithiation, the number of layers that always remain open during cycling increases. As the particle surface in this area will not expand any more, the loss of active lithium decreases again. Figure 7b represents the SOC range 75–95%. Only a small surface area fluctuates between Stage I and Stage II.

The different capacity loss of the cells cycled in the SOC ranges 5–25% und 25–45% can be explained by the same effect, regarding Stage III. The SOC range 5–25% included Stage III (equivalent to the SOC range 45–65% and Stage II) and lost less capacity than the cell cycled slightly above Stage III in the SOC range 25–45% (equivalent to the SOC range 65–85% and Stage II). Because at Stage III only two out of twelve graphite layers need to be opened to further lithiate the anode, the dilation of the particle surface was comparatively small, resulting in a smaller capacity loss than at Stage II.

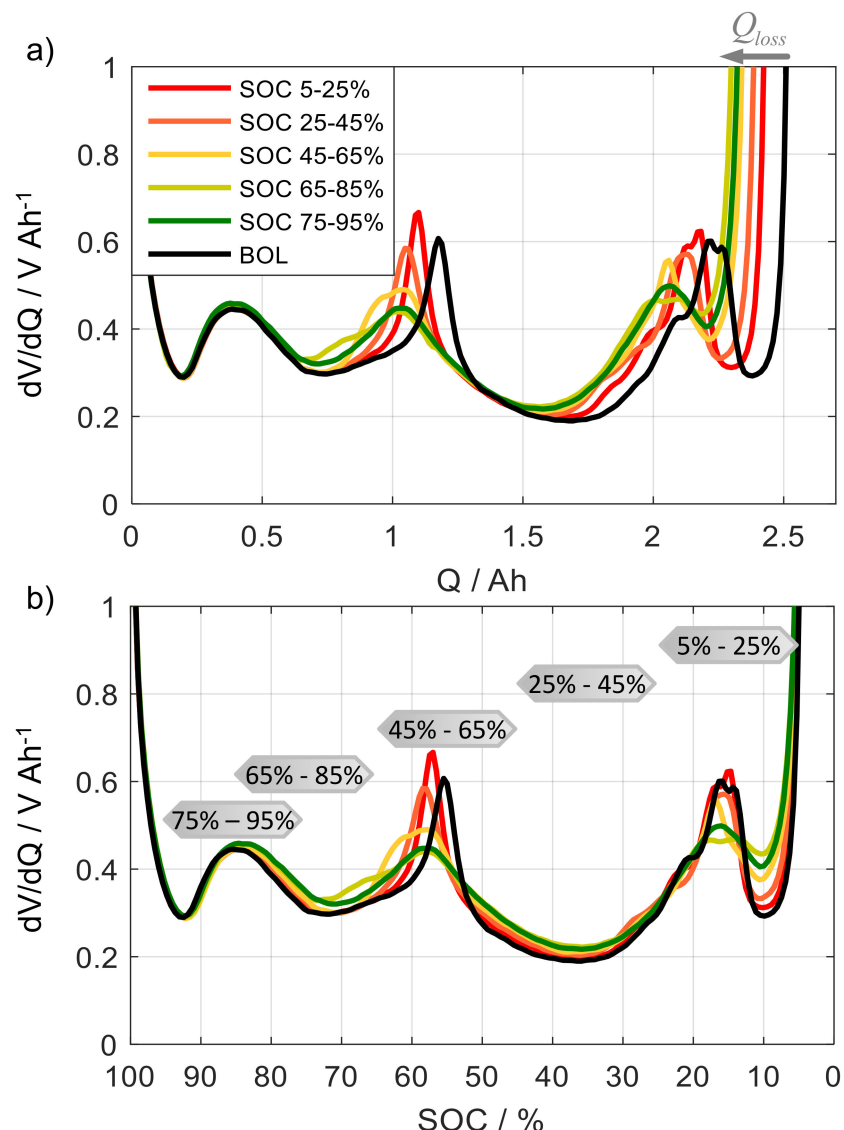


Figure 6. Differential voltage (DV), calculated from the C/40 discharge curves at BOL and at EOT for all cycle-life tests. (a) Differential voltage plotted over the capacity, Q , indicating the capacity loss, Q_{loss} . (b) Differential voltage normalized to the actual remaining capacity, the peak indicating Stage II only shifts slightly to the left during aging.

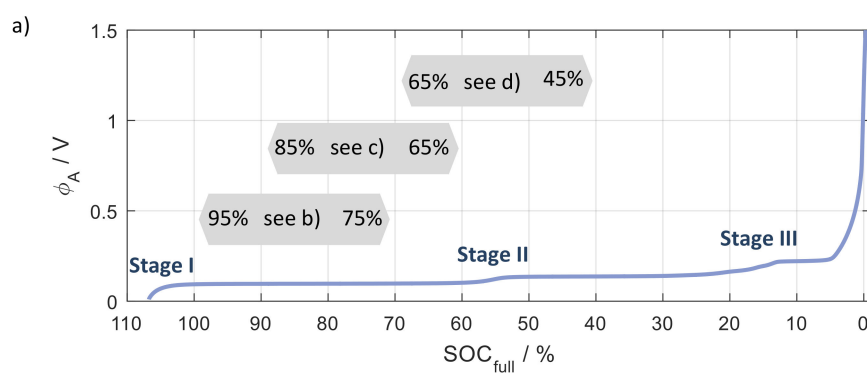


Figure 7. Cont.

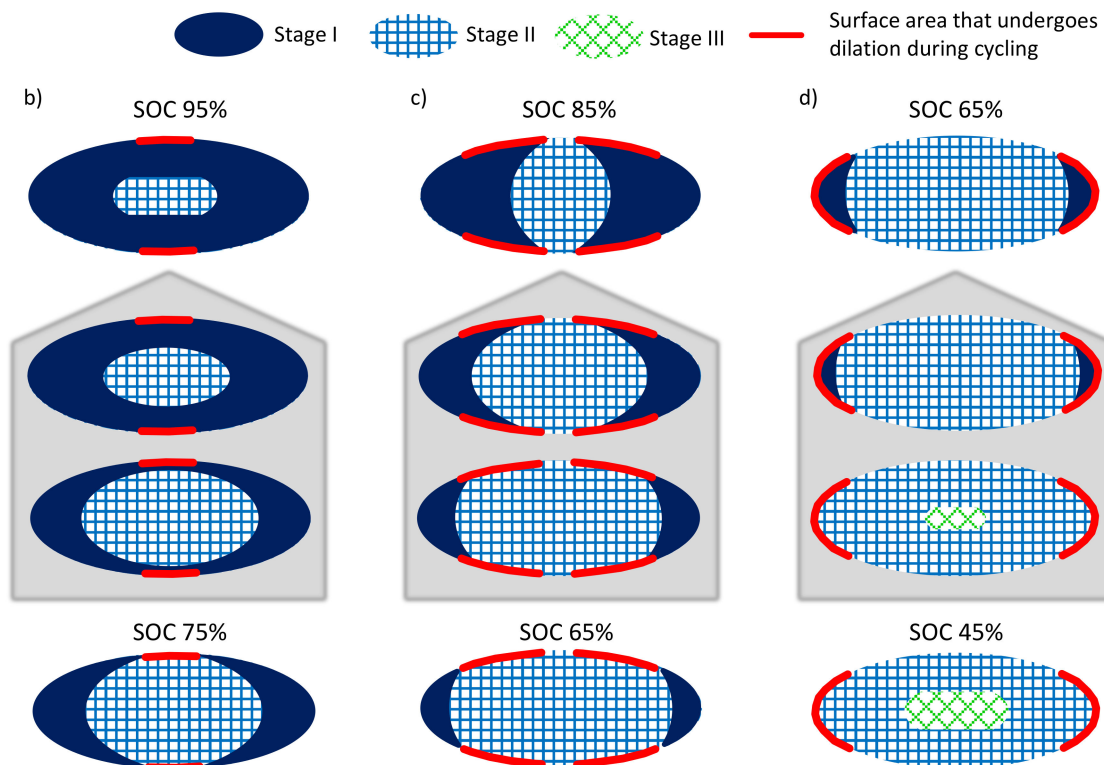


Figure 7. (a) Anode potential and representation of the cycle life experiments in the SOC ranges 45–65%, 65–85%, and 75–95%. (b) Representation of a graphite particle in the SOC range 75–95%. Only a small part of the particle surface suffers from dilation and thus causes new SEI formation. (c) Representation of a graphite particle in the SOC range 65–85%. Much of the particle surface suffers from dilation and thus causes new SEI formation. (d) Representation of a graphite particle in the SOC range 45–65%. Only a small part of the particle surface suffers from dilation and thus causes new SEI formation. The representation of the particles must not be interpreted as a cross-section but figuratively.

4.2. Interpretation of Active Cathode Material Loss, AML_C

The results in Figure 5b show that the active cathode material loss, AML_C , tends to increase with increasing mean SOC. This is in accordance with literature which reports a higher instability of LiCoO₂ in the delithiated state (high full cell SOC) [1,2]. Although doping with Ni and Al improves the stability, this general trend is still visible.

4.3. Practical Importance of the Findings for Cell Design and Load Management

It was found that the active lithium loss restricted the remaining cell capacity and that this loss strongly depended on the SOC range in which the battery was cycled. This finding can help to prolong the battery lifetime in multiple ways: Applying intelligent load management can help to avoid harmful SOC ranges during operation. For example, if an electric device will only be used briefly the next day (and hence, the full cell capacity would not be required), the cell could then be only charged to the SOC of the graphite Stage II. This would avoid a great deal of unnecessary degradation. The position of this stage is especially unfavorable for the current design of the investigated Sony VTC5 cell, because the cell can only be charged up to an SOC of 55% when applying the abovementioned load management (see Figure 8a). To counter this, the choice/development of a graphite material with the stage positioned at higher SOCs could be beneficial or the anode capacity could be increased. This possibility would allow the stage to be positioned at higher SOCs in the full cell. In Figure 8b,c, the cell could be charged up to 80% and 100%, respectively, without passing the stage. Unfortunately, an oversized anode increases battery weight and costs. When the loss of active lithium is the main

cause of capacity fade in a lithium-ion battery, a possible solution would be the insertion of an additional lithium electrode into the cell, which would provide a lithium supply.

The results show, that when applying a battery cell with a graphite anode, it is beneficial to be aware of the position of the potential stages, irrespective of the choice of the cathode material. More generally, it can be stated that whenever an anode material is used, on which SEI is built from electrolyte decomposition, the SOC-dependent dilation should be considered to optimize battery operation. Investigations on the SOC-dependent dilution at different temperatures have not been conducted in this study but might reveal further optimization potential.

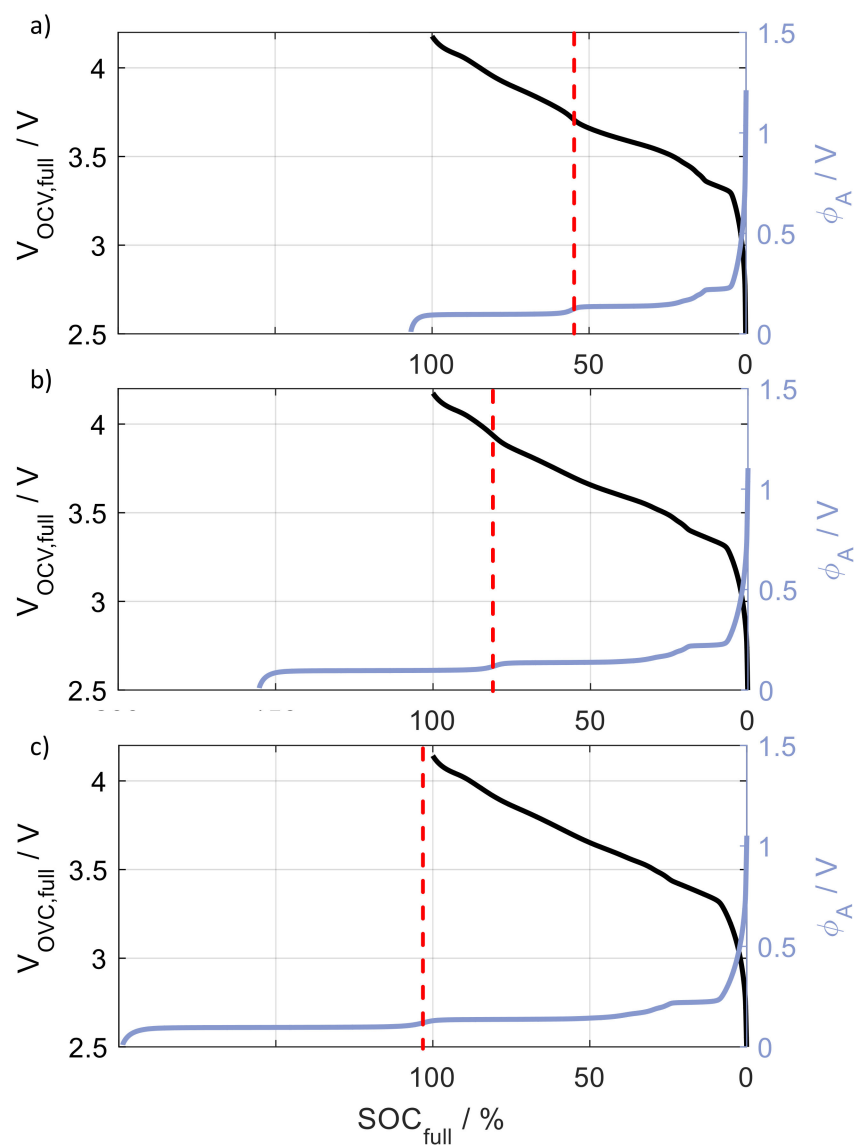


Figure 8. OCV of the Sony VTC5 cell, $V_{OCV,full}$ and OCP of the graphite anode, ϕ_A . (a) Actual balancing. (b) Simulation with slightly oversized anode and (c) with very oversized anode. The SOC of the graphite Stage II is marked with the red dashed lines.

5. Conclusions

A lithium-ion cell with a graphite anode was cycled at different, well-defined SOC ranges (5–25%, 25–45%, 45–65%, 65–85%, and 75–95%) covering different graphite potential ranges. The focus of this test matrix was to experimentally investigate the influence of the graphite stages on the battery's capacity loss (caused by the loss of active lithium which is irreversibly consumed when the SEI is built).

All capacity loss mechanisms (loss of active lithium as well as loss of active electrode material) were quantified with an OCV model. The results show that the loss of active lithium was the dominant cause of capacity fade in each cycle-life test conducted in this work. Over the 4000 test cycles, the cells lost up to 7.5% of active lithium, whereas they only lost up to 3.5% of active anode material and up to 2.5% of active cathode material. Furthermore, the results reveal that cycling the cell in an SOC range slightly above Stage II of the graphite anode resulted in a high loss of active lithium. This can be attributed to the graphite particle surface suffering from high dilation at the threshold between Stages II and I. As a result, the SEI on the surface broke and rebuilt irreversibly consuming active lithium.

Knowing which SOC ranges are especially harmful and cause a high degree of capacity loss can help to prolong the battery lifetime in multiple ways. Applying intelligent load management can help to avoid harmful SOC ranges during operation. Unlike the discharge process (which is controlled by the user and depends on the individual application-specific operating conditions), the charge process can be defined by the manufacturer and adapted to avoid SOC ranges with severe particle surface dilation. For this reason, it is favorable to optimize the cell design in such a way that graphite Stage II is positioned in the edge regions of the SOC range (e.g., at high SOCs) to enable maximum SOC exploitation. The proportions of anode and cathode in a lithium-ion battery or the choice of an appropriate graphite determines the position of the stages in the full cell.

Author Contributions: Conceptualization: M.S., M.W., and S.G.; Methodology: S.G., M.S., and M.W.; Software: M.S. and S.G.; Validation: S.G.; Formal analysis: S.G.; Investigation: S.G.; Resources: E.I.-T.; Data curation: S.G.; Writing—Original draft preparation: S.G.; Writing—Review and editing: M.S., M.W., and E.I.-T.; Visualization: S.G.; Supervision: E.I.-T.; Project administration: E.I.-T.; Funding acquisition: E.I.-T.

Funding: This research was funded by Deutsche Forschungsgemeinschaft (DFG) through projects IV 14/23-1 and GRK 2218/1. We acknowledge support by the KIT-Publication Fund of the Karlsruhe Institute of Technology.

Acknowledgments: Sincere thanks are given to J. Packham for proofreading the manuscript.

Conflicts of Interest: The authors declare no conflict of interest. The funders had no role in the design of the study; in the collection, analyses, or interpretation of data; in the writing of the manuscript, or in the decision to publish the results.

References

1. Vetter, J.; Novák, P.; Wagner, M.R.; Veit, C.; Möller, K.-C.; Besenhard, J.O.; Winter, M.; Wohlfahrt-Mehrens, M.; Vogler, C.; Hammouche, A. Ageing mechanisms in lithium-ion batteries. *J. Power Sources* **2005**, *147*, 269–281. [[CrossRef](#)]
2. Hausbrand, R.; Cherkashinin, G.; Ehrenberg, H.; Gröting, M.; Albe, K.; Hess, C.; Jaegermann, W. Fundamental degradation mechanisms of layered oxide Li-ion battery cathode materials: Methodology, insights and novel approaches. *Mater. Sci. Eng. B* **2015**, *192*, 3–25. [[CrossRef](#)]
3. Stiaszny, B.; Ziegler, J.C.; Krauß, E.E.; Schmidt, J.P.; Ivers-tiffée, E. Electrochemical characterization and post-mortem analysis of aged LiMn_2O_4 - $\text{Li}(\text{Ni}_{0.5}\text{Mn}_{0.3}\text{Co}_{0.2})\text{O}_2$ /graphite lithium ion batteries. Part I: Cycle aging. *J. Power Sour.* **2014**, *251*, 439–450. [[CrossRef](#)]
4. Broussely, M.; Biensan, P.; Bonhomme, F.; Blanchard, P.; Herreyre, S.; Nechev, K.; Staniewicz, R.J. Main aging mechanisms in Li ion batteries. *J. Power Sour.* **2005**, *146*, 90–96. [[CrossRef](#)]
5. Uhlmann, C.; Illig, J.; Ender, M.; Schuster, R.; Ivers-Tiffée, E. In situ detection of lithium metal plating on graphite in experimental cells. *J. Power Sour.* **2015**, *279*, 428–438. [[CrossRef](#)]
6. Zhang, S.S.; Xu, K.; Jow, T.R. Study of the charging process of a LiCoO_2 -based Li-ion battery. *J. Power Sour.* **2006**, *160*, 1349–1354. [[CrossRef](#)]
7. Aurbach, D.; Talyosef, Y.; Markovsky, B.; Markevich, E.; Zinigrad, E.; Asraf, L.; Gnanaraj, J.S.; Kim, H.J. Design of electrolyte solutions for Li and Li-ion batteries: A review. *Electrochim. Acta* **2004**, *50*, 247–254. [[CrossRef](#)]
8. Christensen, J.; Newman, J. A Mathematical Model for the Lithium-Ion Negative Electrode Solid Electrolyte Interphase. *J. Electrochem. Soc.* **2004**, *151*, A1977–A1988. [[CrossRef](#)]
9. Ueda, A.; Ohzuku, T. Solid-State Redox Reactions of LiCoO_2 ($\text{R}3\text{m}$) for 4 Volt Secondary Lithium Cells. *J. Electrochem. Soc.* **1994**, *141*, 2972–2977. [[CrossRef](#)]

10. Nitta, N.; Wu, F.; Lee, J.T.; Yushin, G. Li-ion battery materials: Present and future. *Mater. Today* **2015**, *18*, 252–264. [[CrossRef](#)]
11. Noel, M.; Santhanam, R. Electrochemistry of graphite intercalation compounds. *J. Power Sour.* **1998**, *72*, 53–65. [[CrossRef](#)]
12. Sethuraman, V.A.; Hardwick, L.J.; Srinivasan, V.; Kostecki, R. Surface structural disordering in graphite upon lithium intercalation/deintercalation. *J. Power Sour.* **2010**, *195*, 3655–3660. [[CrossRef](#)]
13. Mercer, M.P.; Otero, M.; Ferrer-Huerta, M.; Sigal, A.; Barraco, D.E.; Hoster, H.E.; Leiva, E.P.M. Transitions of lithium occupation in graphite: A physically informed model in the dilute lithium occupation limit supported by electrochemical and thermodynamic measurements. *Electrochim. Acta* **2019**, *324*, 134774. [[CrossRef](#)]
14. Dubarry, M.; Truchot, C.; Liaw, B.Y. Synthesize battery degradation modes via a diagnostic and prognostic model. *J. Power Sour.* **2012**, *219*, 204–216. [[CrossRef](#)]
15. Schmidt, J.P.; Tran, H.Y.; Richter, J.; Ivers-Tiffée, E.; Wohlfahrt-Mehrens, M. Analysis and prediction of the open circuit potential of lithium-ion cells. *J. Power Sour.* **2013**, *239*, 696–704. [[CrossRef](#)]
16. Fu, R.; Choe, S.Y.; Agubra, V.; Fergus, J. Development of a physics-based degradation model for lithium ion polymer batteries considering side reactions. *J. Power Sour.* **2015**, *278*, 506–521. [[CrossRef](#)]
17. Schindler, S.; Danzer, M.A. A novel mechanistic modeling framework for analysis of electrode balancing and degradation modes in commercial lithium-ion cells. *J. Power Sour.* **2017**, *343*, 226–236. [[CrossRef](#)]
18. Broussely, M.; Herreyre, S.; Biensan, P.; Kasztejna, P.; Nechev, K.; Staniewicz, R.J. Aging mechanism in Li ion cells and calendar life predictions. *J. Power Sour.* **2001**, *97–98*, 13–21. [[CrossRef](#)]



© 2019 by the authors. Licensee MDPI, Basel, Switzerland. This article is an open access article distributed under the terms and conditions of the Creative Commons Attribution (CC BY) license (<http://creativecommons.org/licenses/by/4.0/>).